Materials Science in Semiconductor Processing 135 (2021) 106069

Contents lists available at ScienceDirect

Materials Science in Semiconductor Processing

journal homepage: www.elsevier.com/locate/mssp

Morphological and optical property study of Li doped ZnO produced by microwave-assisted solvothermal synthesis

Patrik Ščajev [a], Ramona Durena [b,c], Pavels Onufrijevs [b,*], Saulius Miasojedovas [a], Tadas Malinauskas [a], Sandra Stanionyte [d], Aleksej Zarkov [e], Anzelms Zukuls [f], Ivita Bite [c], Krisjanis Smits [c]

[a] Institute of Photonics and Nanotechnology, Vilnius University, Sauletekio av. 3, Vilnius, 10257, Lithuania
[b] Institute of Technical Physics, Faculty of Materials Science and Applied Chemistry, Riga Technical University, 3/7 Paula Valdena Str., LV-1048, Riga, Latvia
[c] Institute of Solid State Physics, University of Latvia, Kengaraga 8, LV-1063, Riga, Latvia
[d] Center for Physical Sciences and Technology, Sauletekio av. 3, Vilnius, 10257, Lithuania
[e] Institute of Chemistry, Vilnius University, Naugarduko 24, LT-03225, Vilnius, Lithuania
[f] Research Laboratory of Functional Materials Technologies, Faculty of Materials Science and Applied Chemistry, Riga Technical University, 3/7 Paula Valdena Str., LV-1048, Riga, Latvia

ARTICLE INFO

Keywords:
ZnO
Microwave-assisted Solvothermal Synthesis
Doping
Li
Nanoparticles

ABSTRACT

ZnO materials have been at the centre of many studies for decades. Doping of ZnO by lithium atoms is a prospective approach for compensation of n-type conductivity in the unintentionally doped ZnO aimed at obtaining p-type semiconductor. In this study, we have synthesized ZnO rod-like powders doped with lithium ions (0–0.65 atom%) by the new microwave-assisted solvothermal method in order to obtain greater photoluminescence intensity of ZnO emissions in the UV region. The obtained powders contain nanoparticles from 20 nm up to 250 nm depending on Li content. X-ray diffractometry and Raman spectroscopy were employed to characterise the structure of ZnO powders, scanning electron microscopy was used to determine the morphology, and most importantly the photoluminescence technique was used to investigate the optical properties of the obtained materials. As a result, the photoluminescence intensity has been increased up to an order of magnitude with the Li content in the ZnO crystals. The increase of the excitation laser power has led to an increased carrier lifetime and photoluminescence response intensity that is observed for all the samples.

1. Introduction

Zinc oxide (ZnO) is naturally n-type metal oxide semiconductor with a wide direct band gap of 3.37 eV (at 300 K) and high exciton binding energy of 60 mV, thus the excitons can be observed even at room temperature [1,2]. Combining unique electronic and optical properties with an abundance in the earth's crust, non-toxicity, and high thermal and chemical stability makes ZnO materials suitable for a wide range of applications like gas sensors [3], radiation detectors [4], optoelectronic devices [5], smart windows [6], light-emitting diodes (LEDs) [7], transparent electrodes [8], solar cells [9], etc. More importantly, ZnO application is determined by particle size, shape, aspect ratio, specific surface area, and surface chemistry [10]. Many modification methods have been explored to optimize ZnO material properties and expand its applications [11]. Some of these methods include shape and size control by varying preparation techniques [12,13] and structural modification by doping with different elements [14]. ZnO is well suited for the incorporation of a large variety of dopants due to its crystal lattice [1]. A few of the most popular dopants for ZnO include trivalent ions like Ga, Al, In Ref. [15] and monovalent ions like Na, Li, K [14]. Some of the most frequently used ZnO powder preparation techniques include sol-gel method [16], microwave-assisted solvothermal synthesis [17], solvothermal synthesis [15], co-precipitation method [18] etc. Although solvothermal and microwave assisted solvothermal synthesis methods exhibit a similar particle obtaining approach, the microwave assisted solvothermal synthesis method has some considerable advantages compared to the solvothermal method that include sample heating with microwaves instead of conventional methods. Most notable microwave heating advantages include the short time duration of synthesis, heating uniformity with low thermal gradients, the heated material has no direct

* Corresponding author.
E-mail address: onufrijevs@latnet.lv (P. Onufrijevs).

https://doi.org/10.1016/j.mssp.2021.106069
Received 7 December 2020; Received in revised form 9 June 2021; Accepted 2 July 2021
Available online 6 July 2021

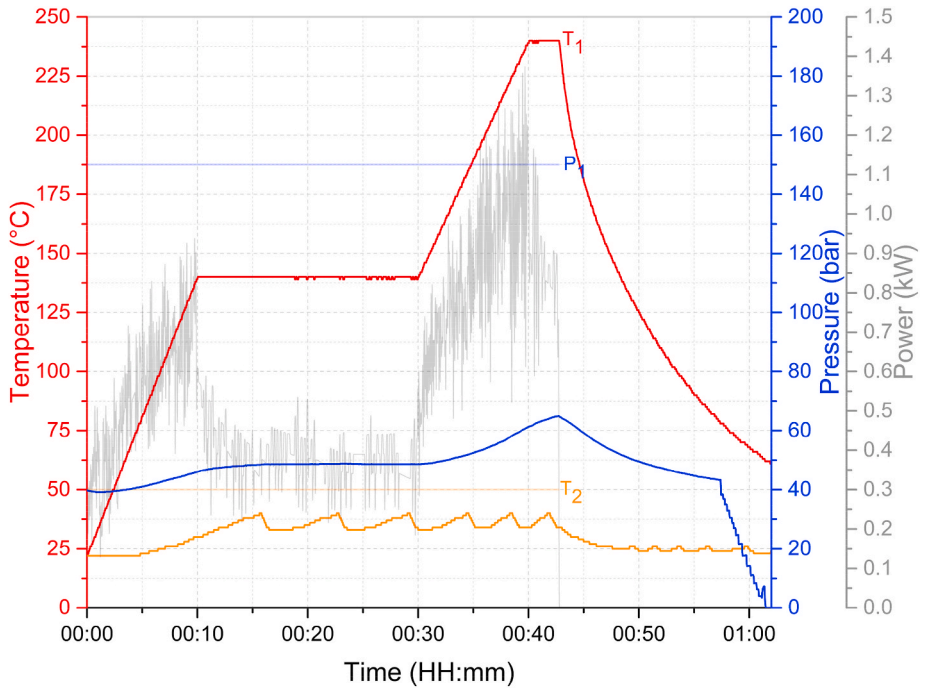

Fig. 1. Microwave-assisted solvothermal synthesis parameters profile for undoped and Li-doped ZnO nanoparticles preparation. T1 is reaction temperature, T2 – upper-temperature limit for the reactor vessel (50 °C), and P1 – upper-pressure limit for the MWST reaction (150 bar).

contact with the heat source, there are no "wall effects" and it offers precise electronic control of the heating process with minimised heat losses [19].

ZnO exhibits a hexagonal wurtzite crystal unit cell structure, and its photoelectrical properties are closely linked with characteristic point defects. ZnO photoluminescence (PL) spectrum consists of two emission bands, one in the UV region from 350 to 400 nm corresponding to exciton near band edge luminescence (NBL), and the other in the visible region from 400 to 800 nm corresponding to defect-related emissions. Although lots of studies have investigated the optical properties in order to determine defect effects, the origin of the visible emission defects is not yet well understood [20].

Undoped ZnO is an n-type semiconductor due to crystal points defects. To overcome this there are two possible variations to obtain p-type conductivity. One variation employs substitution of group-I elements (Li, Na, K) on the Zn-site and other – group-V elements (N, P, Sb) on the O-site [21]. According to Sa´aedi et al. [22], lithium shows the best results from I-group elements. This is due to its small ionic radius of 0.68 Å that is very close to the ionic radius of Zn (0.74 Å) [23]. Lithium can be incorporated in ZnO crystalline lattice in two sites by substituting for Zn^{2+} ion further inducing a hole or by embedding into interstitial sites to form Li^{+} and contributing free electron [24]. Furthermore Lee and Leem [25] suggest that the hole produced by Zn ion substitution with Li ion can compensate the free electron carriers.

In this work, we investigate the structural and optical properties of ZnO powders prepared by the microwave-assisted solvothermal method depending on Li doping ratios. The aim of this work is to obtain greater photoluminescence (PL) intensity of ZnO emissions in the near UV region. ZnO NBL in near UV region is linked with exciton emissions and their decay time is measurable in nanoseconds. Moreover, other studies [26] have shown that Li doped ZnO is a prospective material for obtaining transparent ceramics which can be successfully exploited in various optoelectronic devices.

2. Experimental

Undoped and Li doped ZnO powders were prepared by the microwave-assisted solvothermal synthesis method (MWST). The MWST reaction was performed in a Milestone synthWAVE T660 (Milestone Srl) microwave reactor in an inert atmosphere (N_2, 99,999%). The system was operated at 2.45 GHz frequency with power ranging from 0 to 100% of full power (1.5 kW).

The synthesis started by preparing two solutions (solution A and solution B). Solution A was prepared by dissolving 2 mmol salts in 15 mL absolute ethanol. In this preparation zinc acetate dihydrate ($Zn(Ac)_2 \cdot 2H_2O$, purity $\geq$ 99.5%, Alfa Aesar) and lithium nitrate ($LiNO_3$) were used as salts. The added Li ratios against Zn in the solutions were 0, 0.5, 1, 3, and 5 atom%. Solution B was prepared by dissolving 0.6 g NaOH (purity $\geq$ 98%, Sigma Aldrich) in 30 mL absolute ethanol in a round-bottom flask under reflux condenser whilst vigorously stirring with a magnetic stirrer and heated up to the boiling point of ethanol. When the NaOH and salts were dissolved solution A was added to solution B in a controlled manner. The resulting solution was poured in 70 mL PTFE vial, which was then placed in a Milestone synthWAVE reactor vessel. The exploited heating programme is shown in Fig. 1, where T_1 is reaction temperature, T_2 – upper-temperature limit for the reactor vessel (50 °C), and P_1 – upper-pressure limit for the MWST reaction (150 bar). After heating the obtained particle and solution mixture was cooled down to room temperature. Afterwards, the obtained particles were separated from the solution by centrifugation and washed with methanol for five times and white powders were obtained.

Quantitative determination of Li and Zn in Li-doped ZnO samples was performed by means of inductively coupled plasma optical emission spectrometry (ICP-OES) using a PerkinElmer Optima 7000DV spectrometer. The samples prior to analysis were dissolved in nitric acid (HNO_3, Rotipuran® Supra 69%, Roth) and diluted with deionised water. Calibration solutions were prepared by an appropriate dilution of the standard stock solutions (single-element ICP standards 1000 mg/L, Roth).

Composition of the layers was characterised by X-ray diffraction (XRD), employing a Rigaku SmartLab diffractometer Cu Kα radiation from 9 kW X-ray tube with the rotating anode. The patterns were collected working in Bragg-Brentano focusing geometry using a D/tex Ultra 1D detector in the 2θ range from 30° to 80°.

Table 1
Results of the elemental analysis of the samples, performed by ICP-OES.

Li content in solution (atom%)	Li content in powder (atom%)	Ratio	Doping efficiency, %
0	0	–	–
0.5	0.15	3.3	30.0
1	0.31	3.2	31.0
3	0.54	5.5	18.0
5	0.65	7.7	13.0

Raman analysis was carried out at room temperature using Raman spectrometer Renishaw In-ViaV727 in backscattering geometry. The phonon excitation was performed by green (Ar+, λ = 514.5 nm, grating – 1200 mm^{-1}) laser.

Scanning electron microscope (SEM) images of the samples were obtained using Thermo Fisher Scientific Helios 5 UX operated at 2.00 kV.

ZnO powder luminescence measurements were carried out by powder excitation via a Pharos femtosecond pulsed laser with an Orpheus parametric generator at 10 kHz repetition rate. Excitation conditions were: wavelength 315 nm, spot diameter ~100 μm, maximum excitation power 360 μW.

3. Results and discussion

Powder samples with different Li content were obtained by employing the microwave-assisted solvothermal method. Results of the elemental analysis of the samples performed by ICP-OES are shown in Table 1. It is observed that Li contents in the powders are about three times lower for low Li doping, and up to 8 times lower for 5% solution. That indicates saturation of Li contents in the ZnO lattice. The highest doping efficiencies of 30.0 and 31.0% are obtained for the lowest nominal doping concentrations, 0.5 and 1 atom% Li, respectively. By increasing the nominal doping concentration, the doping efficiency decreases. Similar results are presented by Zhu et al. [27] where Al-doped ZnO thin films were obtained by the sol-gel method and the obtained doping efficiencies for the thin films were between 40 and 15%, decreasing with the increase of the nominal doping concentration.

Obtained SEM images of undoped and Li doped ZnO samples are shown in Fig. 2 (on the right side). As seen in the SEM images, the obtained ZnO powders consist of rod-like and rounded structures. Equivalent diameter distributions obtained from the SEM images are shown in Fig. 2 (on the left side). Basically, particles can be grouped into two groups based on their sizes, larger and smaller particles respectively. The average diameter of the smaller particles varies between 20 and 100 nm, but the larger particles have diameters between 100 and 250 nm. Comparing the undoped sample with Li doped samples, it can be acknowledged that the Li ion doping reduces the size of the obtained ZnO powders. This is in agreement with various published studies [28, 29].

Raman scattering measurements are shown in Fig. 3. Obtained results reveal fundamental vibrational modes of wurtzite structure ZnO rods, that are located at 99 cm^{-1}, 379 cm^{-1}, and 582 cm^{-1} corresponding to E_2 (low), A_1 (TO), E_2 (high) and E_1 (LO) phonon modes respectively [30]. Additional multiphonon process modes are observed at 332 cm^{-1} and 1150 cm^{-1} (not shown in spectra). According to Kirste et al. [31], the Raman components of the surface lithium in the LiO_2 form should be located at 735 cm^{-1} and 1090 cm^{-1}, corresponding to Li–O and O–O vibrations. In our case these vibrational modes were not present, indicating Li is incorporated in the ZnO lattice. Moreover, the intensity of E_1 (LO) phonon mode at 582 cm^{-1} increases with Li content in ZnO. This mode in ZnO is related to the defects such as V_O or Zn_i or their complexes [32,33] and usually the intensity of E_1 (LO) mode in Li doped ZnO is much higher than that of undoped ZnO [34]. Raman peak asymmetric broadening can be related to surface bond contraction and/or the quantum confinement [35].

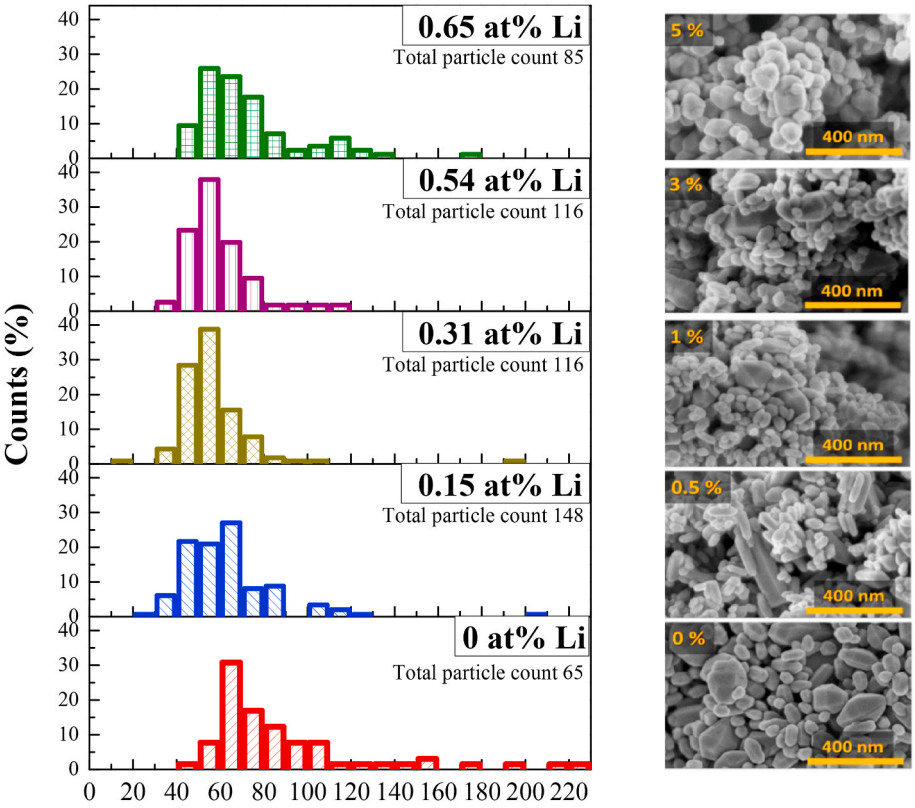

Fig. 2. Equivalent diameter distribution (on the left side), which were obtained from SEM images (on the right side) of ZnO powders undoped and doped with 0.15, 0.31, 0.54, and 0.65 atom% Li.

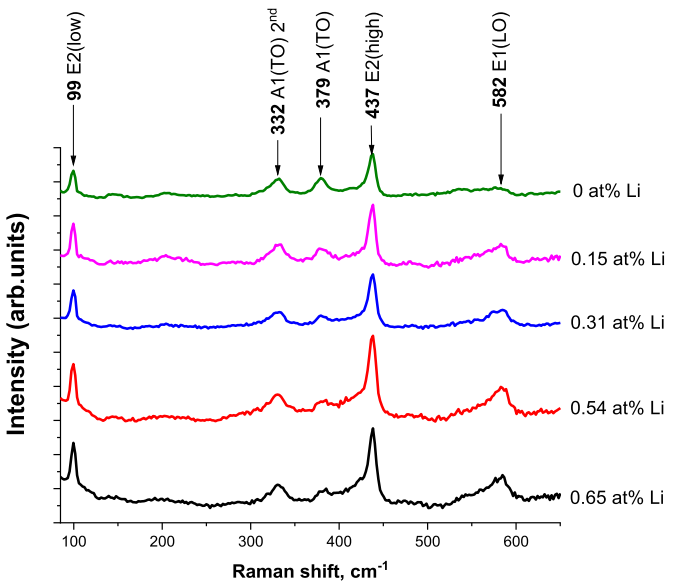

Fig. 3. Raman spectra of undoped and Li doped ZnO with different Li content.

X-ray diffraction measurements of different amount Li doped ZnO crystals are shown in Fig. 4. The obtained samples show a hexagonal (wurtzite) ZnO crystal structure (space group $P6_3mc$) [36]. No other crystalline phase diffraction peaks are present. From the diffraction peaks the broadening crystallite size of ZnO was calculated (Fig. 4). XRD results show the same crystallite size tendency as obtained by SEM investigation, but the measured crystallite size values are systematically smaller. XRD broadening is also affected by crystalline defects, and provide the sizes of defect-free crystallites, which are smaller than the actual crystallites. XRD data confirms that doping with Li reduces crystallite size for all investigated doping concentration, but this effect becomes smaller when the Li concentration increases. Doping with Li does not significantly change peak positions of ZnO (as seen in the insertion of Fig. 4a) as the Li concentration is rather small. With 0.5 atom% Li doping, the strain decreases indicating reduced density of crystalline defects as proposed in Ref. [37] where undoped and Li doped (0, 0.003 and 0.3 wt%) thin films were investigated. But as the Li doping levels increase, so does the strain, indicating higher amounts of Li lattice distortion [23]. Strain calculations in our samples were done by the Williamson-Hall method. We detected <0.1% peak position shift to larger values with increasing Li content, verifying the small Li doping. A similar situation was observed in Ref. [23].

From photoluminescence decay measurements shown in Fig. 5, we can observe that the photoluminescence intensity increases by an order of magnitude with Li content in ZnO crystals. Increasing the power of the laser increases the carrier lifetime and the obtained photoluminescence response intensity for all the samples. The latter can be attributed to saturation of defects. The Li ion amount increase slows down the decay time of emission, resulting in an additional 0.2–0.4 ns delay compared to pure ZnO powder. The excitation peak is more pronounced with higher Li ion content located at 380 nm, and similar findings were produced in Ref. [38] where the ZnO thin film was obtained by the sol-gel spin--coating technique. The PL peak in the near UV region intensity increased with Li doping up to nominal 4 aomt%. Li doping reveals an improvement of recombination properties, due to Li-caused defects. Li doped ZnO is found to be dominated by both Li_i and Li_{Zn} defects where Li_{Zn} complexes with donor defects $(Li_{Zn}OH_O)^{\times}$ and $(Li_{Zn}Li_i)^{\times}$, forming less active defects and reducing n-type conductivity [39,40]. Also, Li_i shifts the Fermi level to mid-gap thus reducing V_{Zn} density [39], which is detrimental to the carrier lifetime [41]. Moreover, most likely Li_i could form a complex with detrimental V_o, similarly as Zn_i-V_o complexes form [42]. PL lifetimes in the studied samples approach that determined in Li-doped hydrothermal ZnO monocrystal, 200 ps [43].

Slow decays in Fig. 6 are superimposed from fast shallow near-bandgap defects and slow deep defect PL emissions. At increased excitation deep defects are saturated leading to faster decay. The defects can be related to the donor-acceptor states.

As shown in Fig. 7a, the decay time of emission at 360–400 nm range increases up to 2 times by increasing Li doping concentration. From Fig. 7b we can observe that the luminescence obtained in the range from 350 nm to 450 nm consists of two components with peaks at 380 nm and 425 nm. The peak at 380 nm could be associated with near band edge luminescence due to the decay of excitons, but the second peak at 425 nm could be assigned to isolated shallow V_{Zn} acceptors induced by Li doping according to findings in Ref. [44]. As the doping concentration increases, the intensity of the 380 nm peak increases, as a result of which the second peak at 425 nm is no longer resolvable for samples with the highest Li concentrations. Also, a much larger PL intensity peak value is obtained at Li > 0.15 atom%.

In Fig. 8a PL intensity dependences on excitation power for undoped and Li doped samples are shown. From this data we can observe that the function consists of 2 components. By applying Li doping, the intensity increase profile changes depending on the excitation energy. In samples containing Li ions the 1-st component intensity is decreased, but the 2nd component intensity increases with Li ion content increase. This may indicate a few times reduction of background doping n_0 as at low excitations PL ~ $Bn_0\Delta N$, while at high excitations PL ~ $B\Delta N^2$, where B is the bimolecular radiative recombination coefficient and ΔN is the excited carrier density. Larger peak PL intensity at Li > 0.5 atom% indicates a plausible improvement of the B coefficient by suppression of carrier capture by defects, supported by a reduced sub-bandgap emission (Fig. 7b). That sub-bandgap emission can be related to donor-acceptor

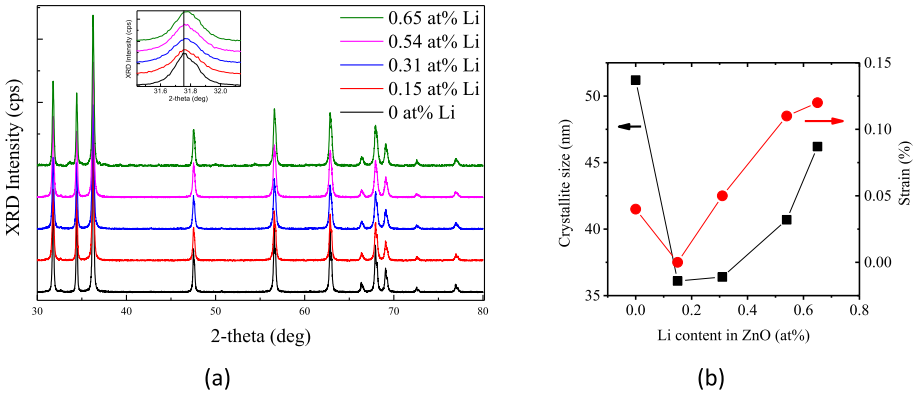

Fig. 4. (a) XRD 2-theta scans for undoped and Li doped ZnO. Peaks indicated correspond to Zincite syngony of ZnO (PDF card 04-008-8197). (b) Crystallite size and strain dependences on Li doping, determined by XRD.

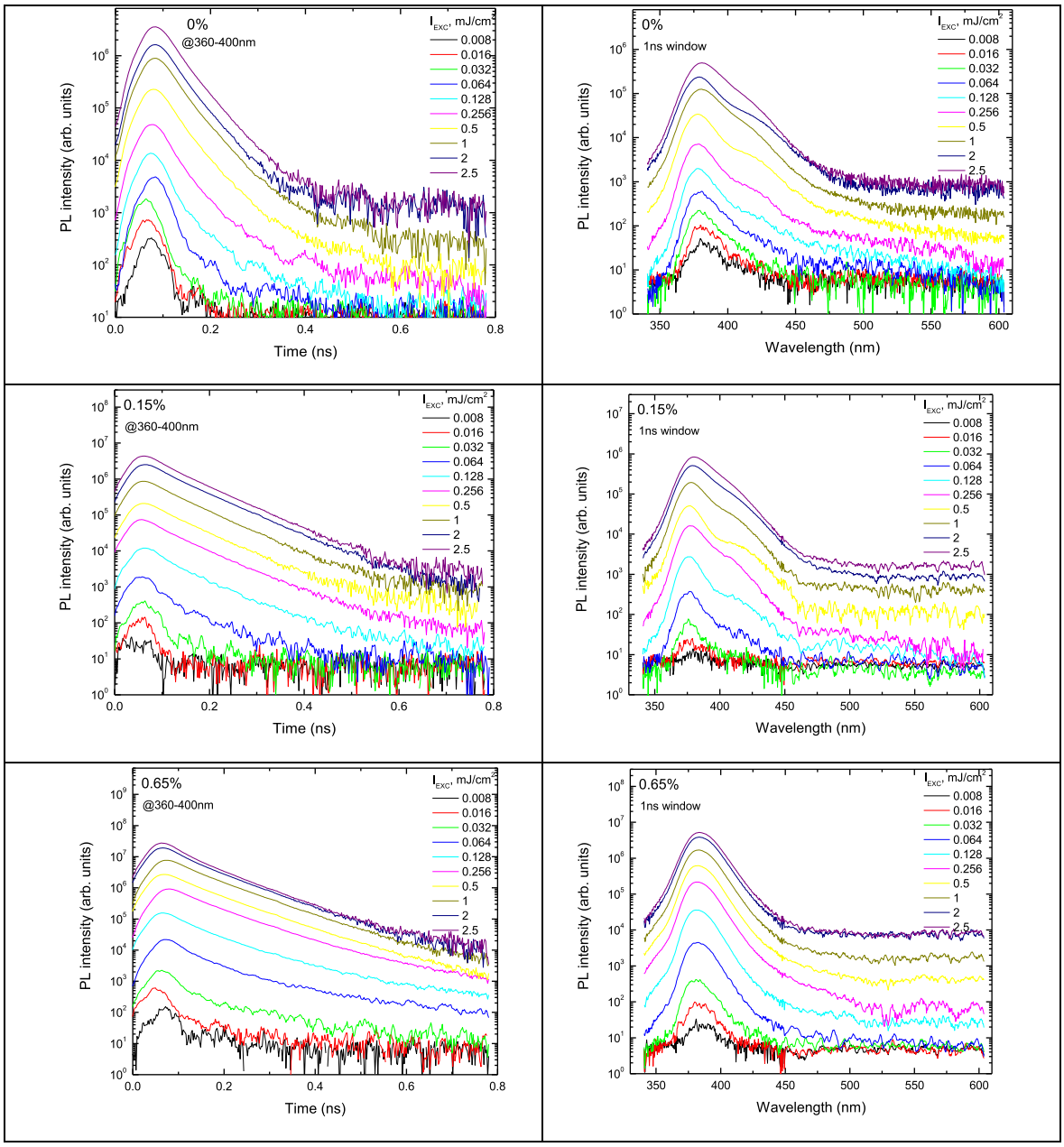

Fig. 5. The decay kinetics at 360–400 nm region and PL spectra of undoped and Li doped ZnO measured at 1 ns window. Lithium concentration in samples is 0–0.65 atom%.

recombination [43]. In Fig. 8b, a slight redshift of emission peak was observed due to lithium incorporation, which is typical for Li doped ZnO [23].

Data portrayed in Fig. 8c reveals that at low excitation energies, FWHM does not correlate with the doping concentration due to defect band admixing, whereas with increasing excitation energy, FWHM converges to one value for all samples of ZnO, regardless of the degree of doping, indicating the weak impact of Li doping on the ZnO lattice structure and hence electronic band structure. On the other hand, the sol-gel method provides a reduction of the bandgap emission and an increase of defect emission with Li doping [45,46], revealing the advantages of our method for high quality ZnO powder preparation.

4. Conclusions

We produced Li doped ZnO powder samples with the new microwave-assisted solvothermal method. The particle size of the obtained powders varies between 20 nm and 250 nm and the size is decreased for samples with Li doping. As a result, the photoluminescence intensity is increased with Li content in ZnO crystals (by an order of magnitude). Increasing the power of the laser increases the carrier lifetime and the obtained photoluminescence response intensity that is observed for all the samples. This elucidates the advance of our method with respect to sol-gel, where the reduction of bandgap emission is observed with Li doping. Our advantage can be explained by the reduction of detrimental to carrier recombination V_{Zn} and V_O defect concentrations by Fermi level shift to the bandgap centre by Li doping, and the formation of Li_{Zn} complexes with V_O.

CRediT author statement

Patrik Ščajev: Conceptualization, Resources, Writing - Original Draft,

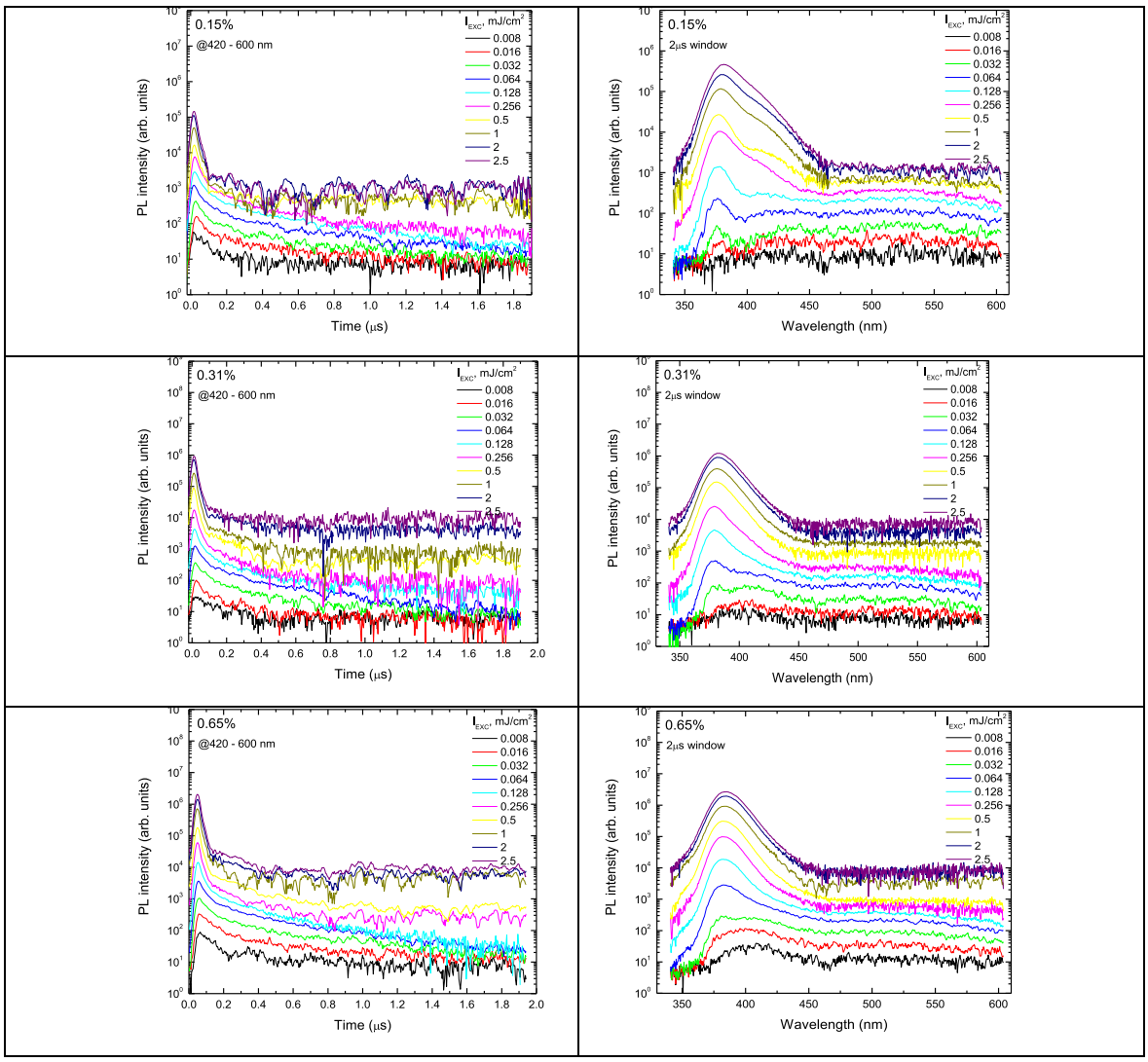

Fig. 6. The decay kinetics at 420–600 nm region and PL spectra of Li doped ZnO measured at 2 μs window. Lithium concentration in samples is 0.15, 0.31, and 0.65 atom%.

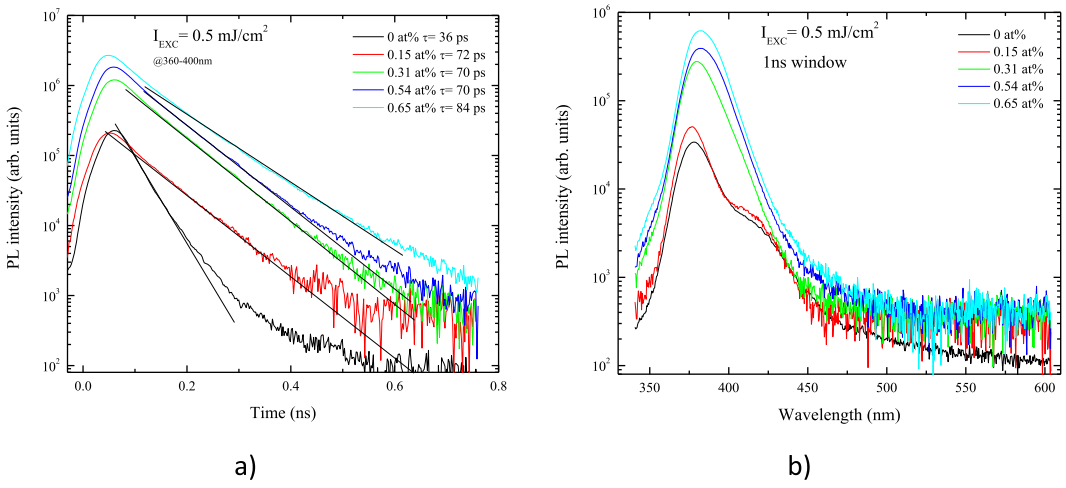

Fig. 7. The PL decay time at 360–400 nm emission range and excitation power 1600 nW (a) and comparison of undoped and Li doped ZnO sample PL spectra intensities (b) at excitation intensity 0.5 mJ/cm^2.

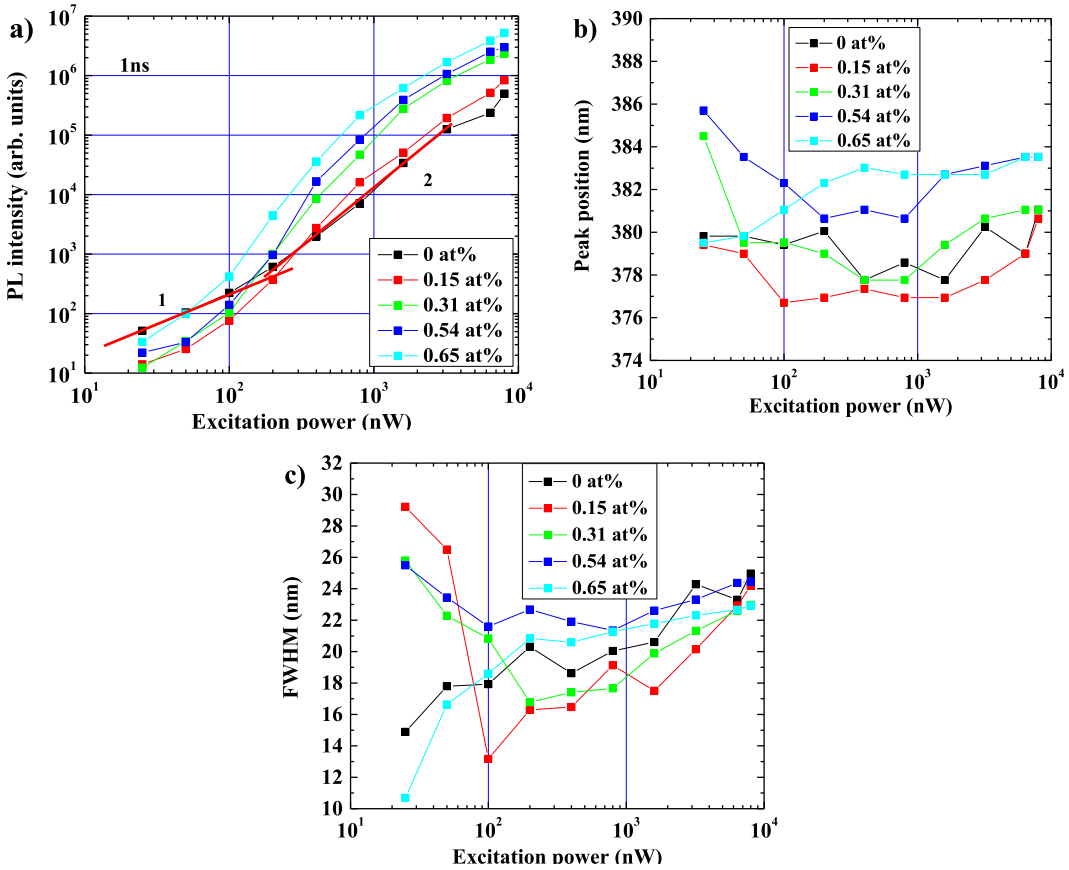

Fig. 8. a) PL intensity; b) peak position and c) FWHM dependence on excitation power of undoped and Li doped ZnO samples.

Supervision, Project administration, Investigation, Visualization, Writing - Review & Editing. Ramona Durena: Writing - Original Draft, Funding acquisition, Investigation, Visualization, Writing - Review & Editing. Pavels Onufrijevs: Conceptualization, Writing - Original Draft, Supervision, Investigation, Visualization, Writing - Review & Editing. Saulius Miasojedovas: Writing - Original Draft, Investigation, Visualization. Tadas Malinauskas: Writing - Original Draft, Investigation, Visualization, Writing - Review & Editing. Sandra Stanionyte: Writing - Original Draft, Investigation, Visualization. Anzelms Zukuls: Writing - Original Draft, Investigation, Writing - Review & Editing. Ivita Bite: Resources, Writing - Original Draft, Funding acquisition, Investigation, Visualization, Writing - Review & Editing. Krisjanis Smits: Resources, Investigation, Visualization.

Declaration of competing interest

The authors declare that they have no known competing financial interests or personal relationships that could have appeared to influence the work reported in this paper.

Acknowledgements

This project has received funding from the Research Council of Lithuania (LMTLT), agreement No *S-M*-ERA.NET-19-2. Ramona Durena acknowledges the financial support provided by Scientific Research Project for Students and Young Researchers Nr. SJZ/2019/6 realized at the Institute of Solid State Physics, University of Latvia is gratefully acknowledged. Ivita Bite acknowledges Institute of Solid State Physics, University of Latvia as the Center of Excellence has received funding from the European Union's Horizon 2020 Framework Programme H2020-WIDESPREAD-01-2016-2017-TeamingPhase2 under grant agreement No. 739508, project CAMART^2 as well as L'ORÉAL Baltic "For Women In Science" Program with the support of the Latvian National Commission for UNESCO and the Latvian Academy of Sciences.

References

[1] A. Zukuls, R. Eglītis, T. Käämbre, R. Ignatans, K. Šmits, K. Rubenis, D. Začs, A. Šutka, Permanent photodoping of plasmonic gallium-ZnO nanocrystals, Nanoscale 12 (2020) 6624–6629, https://doi.org/10.1039/D0NR01005G.
[2] N. Deka, P. Chakraborty, D. Chandra Patra, S. Dhar, S.P. Mondal, Self-powered broadband photodetection using PbS decorated ZnO nanorods/reduced graphene oxide junction, Mater. Sci. Semicond. Process. 118 (2020) 105165, https://doi.org/10.1016/j.mssp.2020.105165.
[3] S. Manohar, X. Zhang, T.M. Swager, K.N. Salama, Recent Progress and Perspectives of Gas Sensors Based on Vertically Oriented ZnO Nanomaterials, vol. 270, 2019, pp. 1–27, https://doi.org/10.1016/j.cis.2019.05.006.
[4] J. Ji, A.M. Colosimo, W. Anwand, L.A. Boatner, A. Wagner, P.S. Stepanov, T. T. Trinh, ZnO Luminescence and Scintillation Studied via Photoexcitation , X-Ray Excitation , and Gamma-Induced Positron Spectroscopy, 2016, pp. 1–9, https://doi.org/10.1038/srep31238.
[5] P. Singh, R. Kumar, R.K. Singh, Progress on Transition Metal-Doped ZnO Nanoparticles and its Application, 2019, https://doi.org/10.1021/acs.iecr.9b01561.
[6] V.O. Zno, High Performance and Enhanced Durability of Thermochromic High Performance and Enhanced Durability of Thermochromic Films Using VO 2 @ ZnO Core-Shell Nanoparticles, 2017, https://doi.org/10.1021/acsami.7b08889.
[7] C. Klingshirn, J. Fallert, H. Zhou, J. Sartor, C. Thiele, F. Maier-Flaig, D. Schneider, H. Kalt, 65 years of ZnO research - old and very recent results, Phys. Status Solidi 247 (2010) 1424–1447, https://doi.org/10.1002/pssb.200983195.
[8] V. Kumar, O.M. Ntwaeaborwa, T. Soga, V. Dutta, H.C. Swart, Rare Earth Doped Zinc Oxide Nanophosphor Powder : A Future Material for Solid State Lighting and Solar Cells, 2017, pp. 2613–2637, https://doi.org/10.1021/acsphotonics.7b00777.
[9] L.F.G. Larsson, G.A.R. Maia, G.T. Tractz, T.L. Valério, D.C.S. Oliszeski, R. Helleis, M.T. da Cunha, P.R.P. Rodrigues, E. do P. Banczek, Application of zinc oxide in hybrid solar cells using a P3HT and P3OT polymer junction as charge carrier, Mater. Res. 22 (2019), https://doi.org/10.1590/1980-5373-mr-2018-0820.
[10] D. Cao, X. Shu, D. Zhu, S. Liang, M. Hasan, S. Gong, Lipid-coated ZnO nanoparticles synthesis, characterization and cytotoxicity studies in cancer cell, Nano Converg 7 (2020) 14, https://doi.org/10.1186/s40580-020-00224-9.
[11] F.-R. Wang, C.-X. Luo, X.-Y. Zhang, J.-K. Liu, X.-H. Yang, Mass-production route and application of ZnO nanocrystals modified with various elements (Li, Al, N, and

P), Res. Chem. Intermed. 42 (2016) 6209–6220, https://doi.org/10.1007/s11164-016-2455-5.
[12] J. Wojnarowicz, T. Chudoba, I. Koltsov, S. Gierlotka, S. Dworakowska, W. Lojkowski, Size control mechanism of ZnO nanoparticles obtained in microwave solvothermal synthesis, Nanotechnology 29 (2018), 065601, https://doi.org/10.1088/1361-6528/aaa0ef.
[13] J. Wojnarowicz, T. Chudoba, S. Gierlotka, K. Sobczak, W. Lojkowski, Size control of cobalt-doped zno nanoparticles obtained in microwave solvothermal synthesis, Crystals 8 (2018) 1–18, https://doi.org/10.3390/cryst8040179.
[14] R. Yousefi, A.K. Zak, F. Jamali-Sheini, The effect of group-I elements on the structural and optical properties of ZnO nanoparticles, Ceram. Int. 39 (2013) 1371–1377, https://doi.org/10.1016/j.ceramint.2012.07.076.
[15] A. Zukuls, R. Eglītis, T. Käämbre, M. Kook, V. Kisand, M. Maiorov, R. Ignatans, R. F. Duarte, M. Järvekülg, A. Šutka, Magnetic and optical properties in degenerated transition metal and Ga co-substituted ZnO nanocrystals, J. Alloys Compd. 805 (2019) 1191–1199, https://doi.org/10.1016/j.jallcom.2019.07.197.
[16] K. Al Abdullah, S. Awad, J. Zaraket, C. Salame, Synthesis of ZnO nanopowders by using sol-gel and studying their structural and electrical properties at different temperature, Energy Procedia 119 (2017) 565–570, https://doi.org/10.1016/j.egypro.2017.07.080.
[17] S. Aksoy, O. Polat, K. Gorgun, Y. Caglar, M. Caglar, Li doped ZnO based DSSC: characterization and preparation of nanopowders and electrical performance of its DSSC, Phys. E Low-Dimensional Syst. Nanostructures. 121 (2020) 114127, https://doi.org/10.1016/j.physe.2020.114127.
[18] R.E. Adam, G. Pozina, M. Willander, O. Nur, Synthesis of ZnO nanoparticles by co-precipitation method for solar driven photodegradation of Congo red dye at different pH, Photonics Nanostructures - Fundam. Appl 32 (2018) 11–18, https://doi.org/10.1016/j.photonics.2018.08.005.
[19] J. Wojnarowicz, T. Chudoba, W. Lojkowski, A review of microwave synthesis of zinc oxide nanomaterials: reactants, process parameters and morphologies, Nanomaterials 10 (2020) 1086, https://doi.org/10.3390/nano10061086.
[20] J. Hua, Q. Wei, Y. Du, X. Yuan, J. Wang, J. Zhao, H. Li, Controlling electron transfer from photoexcited quantum dots to Al doped ZnO nanoparticles with varied dopant concentration, Chem. Phys. Lett. 692 (2018) 178–183, https://doi.org/10.1016/j.cplett.2017.12.039.
[21] K. Meziane, A. Elhichou, A. Elhamidi, A. Almaggoussi, M. Chhiba, Synthesis of lithium doped zinc oxide by sol gel, J. Phys. Conf. Ser. 758 (2016), 012019, https://doi.org/10.1088/1742-6596/758/1/012019.
[22] A. Sa´aedi, R. Yousefi, F. Jamali-Sheini, M. Cheraghizade, A.K. Zak, N.M. Huang, Optical properties of group-I-doped ZnO nanowires, Ceram. Int. 40 (2014) 4327–4332, https://doi.org/10.1016/j.ceramint.2013.08.100.
[23] K. Meziane, A. El Hichou, A. El Hamidi, M. Chhiba, A. Bourial, A. Almaggoussi, Li concentration dependence of structural properties and optical band gap of Li-doped ZnO films, Appl. Phys. A 123 (2017) 430, https://doi.org/10.1007/s00339-017-1039-6.
[24] X. Zhu, Q. Xie, H. Tian, M. Zhang, Z. Gou, S. He, P. Gu, H. Wu, J. Li, D. Yang, High photoresponse sensitivity of lithium-doped ZnO (LZO) thin films for weak ultraviolet signal photodetector, J. Alloys Compd. 805 (2019) 309–317, https://doi.org/10.1016/j.jallcom.2019.07.074.
[25] W. Lee, J.-Y. Leem, Ultraviolet photoresponse properties of Li-doped ZnO thin films prepared by sol–gel spin-coating method, J. Nanosci. Nanotechnol. 17 (2017) 5697–5700, https://doi.org/10.1166/jnn.2017.14143.
[26] B. Xiao, Z. Ye, Y. Zhang, Y. Zeng, L. Zhu, B. Zhao, Fabrication of p-type Li-doped ZnO films by pulsed laser deposition, Appl. Surf. Sci. 253 (2006) 895–897, https://doi.org/10.1016/j.apsusc.2006.01.041.
[27] M.W. Zhu, H.B. Ma, P.H. Jin, Y.N. Jin, N. Jia, H. Chen, C.Z. Liu, An insight into the low doping efficiency of Al in sol–gel-derived ZnO:Al films: role of the dopant chemical state, Appl. Phys. Mater. Sci. Process 126 (2020) 1–9, https://doi.org/10.1007/s00339-020-03670-8.
[28] M.M. Hassan, W. Khan, A. Azam, A.H. Naqvi, Effect of size reduction on structural and optical properties of ZnO matrix due to successive doping of Fe ions, J. Lumin. 145 (2014) 160–166, https://doi.org/10.1016/j.jlumin.2013.06.024.
[29] N.R. Yogamalar, A. Chandra Bose, Burstein-Moss shift and room temperature near-band-edge luminescence in lithium-doped zinc oxide, Appl. Phys. Mater. Sci. Process 103 (2011) 33–42, https://doi.org/10.1007/s00339-011-6304-5.
[30] R. Zhang, P.-G. Yin, N. Wang, L. Guo, Photoluminescence and Raman scattering of ZnO nanorods, Solid State Sci. 11 (2009) 865–869, https://doi.org/10.1016/j.solidstatesciences.2008.10.016.
[31] R. Kirste, Y. Aksu, M.R. Wagner, S. Khachadorian, S. Jana, M. Driess, C. Thomsen, A. Hoffmann, Raman and photoluminescence spectroscopic detection of surface-bound Li+O2− defect sites in Li-doped ZnO nanocrystals derived from molecular precursors, ChemPhysChem 12 (2011) 1189–1195, https://doi.org/10.1002/cphc.201000852.
[32] D.-F. Zhang, L.-D. Sun, C.-H. Yan, Optical properties of ZnO nanoplatelets and rectangular cross-sectioned nanowires, Chem. Phys. Lett. 422 (2006) 46–50, https://doi.org/10.1016/j.cplett.2006.02.026.
[33] A. Zhao, T. Luo, L. Chen, Y. Liu, X. Li, Q. Tang, P. Cai, Y. Qian, Synthesis of ordered ZnO nanorods film on zinc-coated Si substrate and their photoluminescence property, Mater. Chem. Phys. 99 (2006) 50–53, https://doi.org/10.1016/j.matchemphys.2005.10.013.
[34] Q. Wang, J. Zhang, S. Yang, J. Jiang, Z. Song, D. Xu, J. Li, Y. Sun, Enhancement of multi-photon Raman scattering and photoluminescence emission from Li-doped ZnO nanowires, J. Phys. Commun. 3 (2019), 015006, https://doi.org/10.1088/2399-6528/aafb7f.
[35] Y. Gao, P. Yin, Origin of asymmetric broadening of Raman peak profiles in Si nanocrystals, Sci. Rep. 7 (2017) 43602, https://doi.org/10.1038/srep43602.
[36] M. Vaseem, A. Umar, Y. Hahn, ZnO Nanoparticles : Growth, Properties, and Applications, American Scientific Publishers, 2010.
[37] L. Khomenkova, V. Kushnirenko, M. Osipenok, K. Avramenko, Y. Polishchuk, I. Markevich, V. Strelchuk, V. Kladko, L. Borkovska, T. Kryshtab, Effect of Li-doping on photoluminescence of screen-printed zinc oxide films, MRS Proc 1766 (2015) 167–177, https://doi.org/10.1557/opl.2015.424.
[38] M.S. Aida, M. Hjiri, Temperature-dependent photoluminescence of Li-doped ZnO, J. Mater. Sci. Mater. Electron. 31 (2020) 10521–10530, https://doi.org/10.1007/s10854-020-03600-7.
[39] T.S. Bjørheim, S. Erdal, K.M. Johansen, K.E. Knutsen, T. Norby, H and Li related defects in ZnO and their effect on electrical properties, J. Phys. Chem. C 116 (2012) 23764–23772, https://doi.org/10.1021/jp307835c.
[40] N. Shakti, C. Devi, A.K. Patra, P.S. Gupta, S. Kumar, Lithium doping and photoluminescence properties of ZnO nanorods, AIP Adv. 8 (2018), 015306, https://doi.org/10.1063/1.5008863.
[41] V. Quemener, L. Vines, E.V. Monakhov, B.G. Svensson, Electronic properties of vacancy related defects in ZnO induced by mechanical polishing, Appl. Phys. Lett. 99 (2011) 112112, https://doi.org/10.1063/1.3638470.
[42] D.H. Kim, G.W. Lee, Y.C. Kim, Interaction of zinc interstitial with oxygen vacancy in zinc oxide: an origin of n-type doping, Solid State Commun. 152 (2012) 1711–1714, https://doi.org/10.1016/j.ssc.2012.06.016.
[43] P. Onufrijevs, P. Ščajev, K. Jarašiūnas, A. Medvid, V. Korsaks, N. Mironova-Ulmane, M. Zubkins, H. Mimura, Photo-electrical and transport properties of hydrothermal ZnO, J. Appl. Phys. 119 (2016) 135705, https://doi.org/10.1063/1.4945016.
[44] J. Lv, Y. Liu, Spectroscopic evidence that Li doping creates shallow V Zn in ZnO, Phys. Chem. Chem. Phys. 19 (2017) 5806–5812, https://doi.org/10.1039/C6CP08012J.
[45] W. Hb, D. Wr, B. Zaghouani, M. Mj, Li-doped ZnO sol-gel thin films: correlation between structural morphological and optical properties, J. Textil. Sci. Eng. 8 (2018) 1–7, https://doi.org/10.4172/2165-8064.1000328.
[46] H.-P. Hsu, D.-Y. Lin, C.-Y. Lu, T.-S. Ko, H.-Z. Chen, Effect of lithium doping on microstructural and optical properties of ZnO nanocrystalline films prepared by the sol-gel method, Crystals 8 (2018) 228, https://doi.org/10.3390/cryst8050228.